

# A Novel Regulation Inter-Coupled Control Scheme for Doubly Fed Wind Induction System

Sayed O. Madbouly<sup>1</sup>, Adel M. Sharaf<sup>2\*</sup>

<sup>1</sup>Electric Power and Machines Dept., Ain Shams University, Cairo, Egypt

<sup>2</sup>Sharaf Energy Systems, Inc., Fredericton-NB, Canada

Received: 07 July 2015; Revised: 31 July 2015; Accepted: 08 August 2016; Published: 1 December 2016

Turk J Electrom Energ Vol: 1 No: 2 Page: 8-16 (2016)

SLOI: <http://www.sloi.org/>

\*Correspondence E-mail: [profdransharaf@yahoo.ca](mailto:profdransharaf@yahoo.ca)

**ABSTRACT** The paper presents a novel variable structure coordinated controller for a brushless doubly fed induction generator (BDFG) to improve its dynamic performance. The system under study consists of a BDFG driven variable speed wind turbine. The machine model in d-q power winding (PW) synchronously rotating reference frame is formulated in Matlab/Simulink. The new vector control algorithm which contains two control paths was then developed. The first path controls the active power of the power winding and the other controls its reactive power. The dynamic performance of the BDFG with the new controller has been tested when the overall system is subjected to a various patterns of wind speed. Also the transient and dynamic response is tested under sudden short circuit and open circuit at the generator bus. The digital simulation results showed that the new vector controller improved the dynamic performance of the overall system.

**Keywords:** Wind-brushless doubly fed induction machine, Vector control, Variable structure coordinated controller

**Cite this article:** S.O. Madbouly, A.M. Sharaf, A Novel Regulation Inter-Coupled Control Scheme for Doubly Fed Wind Induction System, Turkish Journal of Electromechanics & Energy 1(2) 8-16 (2016)

## 1. INTRODUCTION

Recently, variable speeds doubly fed generators have been extensively utilized in wind energy applications. They provide the ability of adjusting the wind turbine speed as a function of wind speed in order to maximize the output power [1]. One of these generators is the Doubly Fed Induction Generator (DFIG) which allows the speed variation through the use of bi-directional power converter connected to its rotor [2]. The disadvantages of DFIG are the presence of slip rings and brushes, which need frequent inspections and maintenance. Therefore, the reliability of the overall system is decreased and the maintenance cost is increased [3].

Efforts have been directed towards eliminating the slip rings and brushes while maintaining the benefits of DFIG. In this paper Brushless Doubly Fed Induction Generator (BDFG) is proposed. The construction feature of grid connected BDFG is shown in Figure 1. In this configuration, the stator incorporates two sets of three phase windings with different number of poles. One of them is connected directly to the grid, and is called the Power Winding (PW), since it handles most of machine

power. The other one is connected via a bi-directional converter to the grid, it handles a small percentage of machine power and it is called the Control Winding (CW).

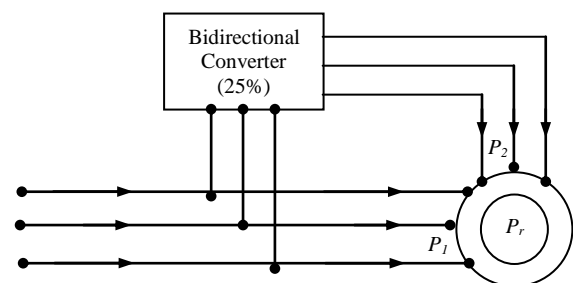


Fig. 1. Configuration of grid connected brushless doubly fed induction machine

The power rating of the converter depends on the adjustable speed range, which is limited in variable speed wind turbines. Therefore, the converter rating is a small percentage of the machine rating [4].

In BDFG the active and the reactive power of the power winding can be controlled through controlling the magnitude; frequency and phase sequence of the applied voltage of the control winding. This can be implemented by using direct torque control technique [5] or vector control schemes [3, 6, 7]. This paper presents a novel vector control of the BDFG which achieves an enhanced decoupled control of active and reactive power of BDFG driven variable speed wind turbine.

## 2. SYSTEM MODELING

The system model is consisting of three main parts.

### 2.1 Wind Turbine Model

The mechanical power output from the wind turbine can be calculated from the following equation:

$$P_m = \frac{1}{2} \rho \pi R_r^2 v_w^3 C_p(\beta, \lambda) \quad (1)$$

Where  $v_w$  is the wind speed,  $\rho$  is the air density,  $R_r$  is the radius of the turbine blades, and  $C_p$  is the power coefficient or performance coefficient which is a function of both the tip speed ratio  $\lambda$ , and the blade pitch angle  $\beta$ . The tip speed ratio  $\lambda$  (TSR) is the ratio between the tip speed and the wind speed. It can be expressed as follows [8, 9];

$$\lambda = \frac{\omega_r \cdot R_r}{v_w} \quad (2)$$

The relation between the power coefficient and both of the tip speed ratio  $\lambda$  and the pitch angle  $\beta$  is approximated by the following equation [10, 11].

$$C_p(\lambda, \beta) = 0.22 \left( \frac{116}{\lambda_i} - 0.4\beta - 5 \right) \cdot e^{-\frac{12.5}{\lambda_i}} \quad (3)$$

Where  $\lambda_i$  is given by:

$$\frac{1}{\lambda_i} = \frac{1}{\lambda + 0.08\beta} - \frac{0.035}{\beta^3 + 1} \quad (4)$$

Figure 2 shows the relation between the performance coefficient and the tip speed ratio at different pitch angle, it can be seen that the maximum performance coefficient is  $C_{pmax}=0.438$  and occurs at a tip speed ratio of  $\lambda_{opt}=6.3$ .

The wind turbine model can be simulated in Matlab/Simulink program as shown in Figure 3 [12, 13].

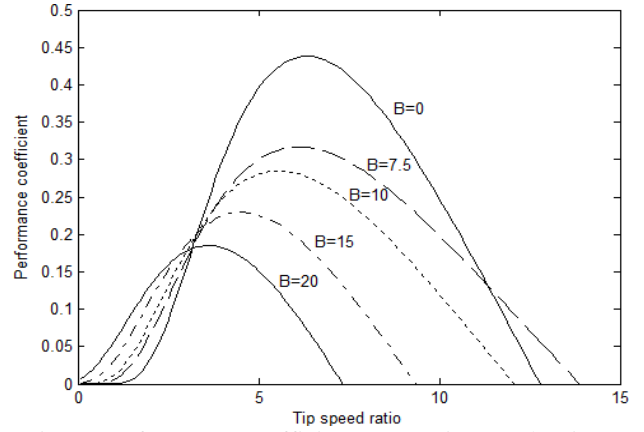


Fig. 2. Performance coefficient versus tip-speed ratio at different pitch angles

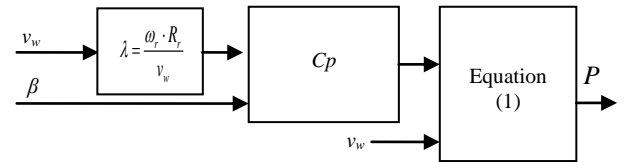


Fig. 3. Wind turbine input- output model

### 2.2 Drive Train Model

The drive train model of the wind turbine is represented by two mass models as shown in Figure 4. The model consists of two main masses, i.e. turbine mass and generator mass. The two masses are connected to each other with a shaft that has a stiffness constant ( $K_s$ ) and damping constant ( $D_s$ ). The input to the drive train model is the aerodynamic torque referred to the generator side (i.e. high speed side) and the output from the model is the generator speed ( $\omega_g$ ). The equations of the drive train are:

$$T_t - K_s \theta_{tg} - D_s \cdot (\omega_t - \omega_g) = J_t \cdot \frac{d\omega_t}{dt} \quad (5)$$

$$K_s \theta_{tg} + D_s \cdot (\omega_t - \omega_g) - T_g = J_g \cdot \frac{d\omega_g}{dt} \quad (6)$$

Where  $T_t$ ,  $J_t$  and  $\omega_t$  are the torque, inertia and speed of the wind turbine referred to the generator side, respectively;  $T_g$ ,  $J_g$  and  $\omega_g$  are the torque, inertia and speed of the generator, respectively; and  $\theta_{tg}$  is the shaft twist angle, which is given by:

$$\frac{d\theta_{tg}}{dt} = (\omega_t - \omega_g) \quad (7)$$

### 2.3 Dynamic Model of BDFG

In order to derive the model of BDFM, the following assumptions are made [14].

- Assume linear magnetic circuit, and neglect saturation.
- Sinusoidal distributed stator winding
- No direct mutual coupling between the power and control winding.

The BDFM equations are derived in the  $d-q$  reference frame which rotates synchronously with the power

winding stator flux by angular speed of  $\omega_r$  (The d- axis is taken to be aligned with the PW flux space vector) [15, 16, 17]. These are:

$$v_p = R_{sp} i_p + \frac{d\psi_p}{dt} + j\omega_1 \psi_p \quad (8)$$

$$\psi_p = L_{sp} i_p + L_{hp} i_r \quad (9)$$

$$v_c = R_{sc} i_c + \frac{d\psi_c}{dt} + j(\omega_1 - (p_1 + p_2)\omega_r) \psi_c \quad (10)$$

$$\psi_c = L_{sc} i_c + L_{hc} i_r \quad (11)$$

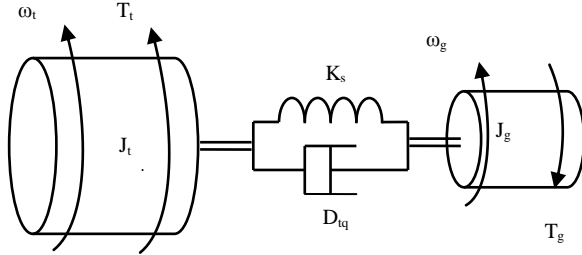


Fig. 4. Drive train model

$$v_r = R_r i_r + \frac{d\psi_r}{dt} + j(\omega_1 - p_1 \omega_r) \psi_r \quad (12)$$

$$\psi_r = L_r i_r + L_{hp} i_p + L_{hc} i_c \quad (13)$$

Where:

- $v_p$ ,  $v_c$  and  $v_r$  are the PW, CW and rotor winding voltage vector respectively.
- $R_{sp}$ ,  $R_{sc}$  and  $R_r$  are the PW, CW and rotor resistances.
- $L_{sp}$ ,  $L_{sc}$  and  $L_r$  are the self-inductances of the PW, CW and rotor winding respectively.
- $L_{hp}$  is the mutual inductance between the PW and the rotor winding and  $L_{hc}$  is the mutual inductance between the CW and the rotor winding.
- $\psi_p$ ,  $\psi_c$  and  $\psi_r$  are the PW, CW and rotor flux space vectors respectively.

The electromagnetic torque can be expressed as the sum of the electromagnetic torques produced by the PW and CW. It can be expressed by the following equation.

$$T_{em} = \frac{3}{2} p_1 \text{Im}[i_p \psi_p^*] + \frac{3}{2} p_2 \text{Im}[i_c \psi_c^*] \quad (14)$$

The power windings active and reactive powers are expressed as:

$$P_p = \frac{3}{2} (v_{pd} i_{pd} + v_{pq} i_{pq}) \quad (15)$$

$$Q_p = \frac{3}{2} (v_{pq} i_{pd} - v_{pd} i_{pq}) \quad (16)$$

### 3. CONTROL STRATEGY OF THE ALL SYSTEM

The control strategy of the overall system can be divided into two parts as following.

#### 3.1 Generator Control Part

The target of this part is to achieve a fully independent control of the active and reactive power of the PW, through the control of the control winding

voltage. This can be fulfilled using the vector control technique as described in the following section.

#### 3.2 PW Power Control

The model of the BDFG is derived in the PW synchronously rotating  $d$ - $q$  reference frame with the  $d$ -axis aligned with the PW flux. Accordingly,  $\psi_{pd} = |\psi_p|$  and there is no component in the  $q$ -axis:

$$\psi_{pq} = 0 \quad \& \quad \psi_{pd} = |\psi_p| \quad (17)$$

Since the PW is connected directly to the grid,  $|\psi_p|$  and  $v_{pd}$  can be considered constant. Consequently, equations (12) and (13) can be simplified as follows:

$$p_p = \frac{3}{2} v_{pq} i_{pq} \quad \text{and} \quad Q_p = \frac{3}{2} v_{pd} i_{pd} \quad (18)$$

It can be seen from (18) that the active and reactive power can be regulated by the  $q$ -component and  $d$ -component of the PW current respectively

#### 3.2.1 PW Current Control

The dynamic relation between the CW and the PW currents is derived in Appendix (A).

$$\frac{di_{cd}}{dt} = \frac{R_r L_{sp}}{L_{hp} L_{hc}} i_{pd} + \frac{\sigma L_r L_{sp}}{L_{hp} L_{hc}} \frac{di_{pd}}{dt} - \frac{R_r}{L_{hp} L_{hc}} |\psi_p| - \frac{\sigma L_r L_{sp} \omega_{sl}}{L_{hp} L_{hc}} i_{pq} + \omega_{sl} i_{cq} \quad (19)$$

$$\frac{di_{cq}}{dt} = \frac{R_r L_{sp}}{L_{hp} L_{hc}} i_{pq} + \frac{\sigma L_r L_{sp}}{L_{hp} L_{hc}} \frac{di_{pq}}{dt} - \frac{L_r \omega_{sl}}{L_{hp} L_{hc}} |\psi_p| + \frac{\sigma L_r L_{sp} \omega_{sl}}{L_{hp} L_{hc}} i_{pd} - \omega_{sl} i_{cd} \quad (20)$$

where;

$$\omega_{sl} = \omega_1 - p_1 \omega_r \quad (21)$$

The first two terms of (19) and (20) represent the direct relation between ( $i_{pd}$  and  $i_{cd}$ ) and ( $i_{pq}$  and  $i_{cq}$ ), respectively while the other terms represent the cross coupling terms which cross couple the  $d$  and  $q$  axis variables (i.e. changing the CW current in one axis affects the PW current not only in this axis but also in the other axis). From (19) and (20) it can be seen that, the PW currents ( $i_{pd}$  and  $i_{pq}$ ) can be linearly controlled by the CW currents ( $i_{cd}$  and  $i_{cq}$ ) respectively after compensating the cross coupling terms by feed forward control action.

#### 3.3 Control of CW Currents

From (8) to (16), the dynamic relation between the CW current and the CW voltage in the  $d$ -axis ( $v_{cd}$  and  $i_{cd}$ ) and  $q$ -axis ( $v_{cq}$  and  $i_{cq}$ ) can be obtained as follows:

$$V_{cq} = R_{sc} i_{cq} + (L_{sc} - \frac{L_{hc}^2}{\sigma L_r}) \frac{di_{cq}}{dt} + \frac{R_r L_{sp} L_{hc}}{\sigma L_{hp} L_r} i_{pq} + [\omega_{sl} (L_{sc} - \frac{L_{hc}^2}{\sigma L_r}) - p_2 L_{sc} \omega_r] i_{cd} + p_2 \omega_r \frac{L_{sp} L_{hc}}{L_{hp}} i_{pd} + \frac{L_{hc}}{L_{hp}} \left( \frac{\omega_{sl} (\sigma - 1)}{\sigma} - p_2 \omega_r \right) |\psi_p| \quad (22)$$

$$V_{cd} = R_{sc} i_{cd} + (L_{sc} - \frac{L_{hc}^2}{\sigma L_r}) \frac{di_{cd}}{dt} + \frac{R_r L_{sp} L_{hc}}{\sigma L_{hp} L_r} i_{pd} - [\omega_{sl} (L_{sc} - \frac{L_{hc}^2}{\sigma L_r}) - p_2 L_{sc} \omega_r] i_{cq} - p_2 \omega_r \frac{L_{sp} L_{hc}}{L_{hp}} i_{pq} - \frac{R_r L_{hc}}{\sigma L_{hp} L_r} |\psi_p| \quad (23)$$

Similar to (19) and (20), it can be seen that the first two terms in (22) and (23) define the direct relation between ( $v_{cd}$  and  $i_{cd}$ ) and ( $v_{cq}$  and  $i_{cq}$ ) respectively. From this relation, it can be seen that, the CW currents ( $i_{cd}$  and  $i_{cq}$ ) can be linearly controlled by the CW voltages ( $v_{cd}$

and  $v_{cq}$ ) respectively. The other terms in (22) and (23) (from the 3<sup>rd</sup> term up to the 6<sup>th</sup> term) represent the cross coupling disturbances between the d and q axes.

3.4 The Proposed Control Scheme

From the previous analysis, the active power of the PW can be controlled by the q-component of the CW voltage, while the reactive power can be controlled by the d-component of the CW voltage as follows:

$$\begin{aligned}
 P_{pw} &\xrightarrow{\text{Controlled}} i_{pq} \xrightarrow{\text{Controlled}} i_{cq} \xrightarrow{\text{Controlled}} v_{cq} \\
 Q_{pw} &\xrightarrow{\text{Controlled}} i_{pd} \xrightarrow{\text{Controlled}} i_{cd} \xrightarrow{\text{Controlled}} v_{cd}
 \end{aligned}$$

The novel controller developed by the second author is a variable structure sliding mode VSC-SMC controller with dual loop inter-coupling of the powers  $P, Q$  tracking loops as shown in Figure 5. The selected (d-q) current references are later input to classical PI inner controllers to derive the d-q command voltages ( $v_{cd}^*, v_{cq}^*$ ) as shown in Figure 6. The use of variable structure outer controller for ( $P_{ref}, Q_{ref}$ ) control loops ensure fast dynamic reference and minimal ripple content due to the insertion of the low pass filter to ( $\sigma_p, \sigma_q$ ) sliding surface slopes.

3.5 Wind Turbine Control Scheme

The target from variable speed wind turbine controller is to maximize the captured power from the wind when the wind speeds below its rated value and limiting the output power at the rated value when the wind speed exceeds its rated value. Two controllers are required to satisfy the previous control strategy.

3.6 Speed Controller

Figure 6 shows the speed controller that the reference speed is compared with the actual speed to get the speed error which is manipulated by a PI controller. The output from the PI controller is the reference active power, which is used by the BDFG controller as mentioned before. The reference speed is determined from the maximum power point tracking curve shown in Figure 7.

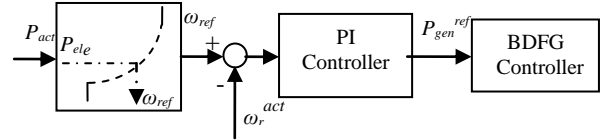


Fig. 6. Block diagram of speed controller

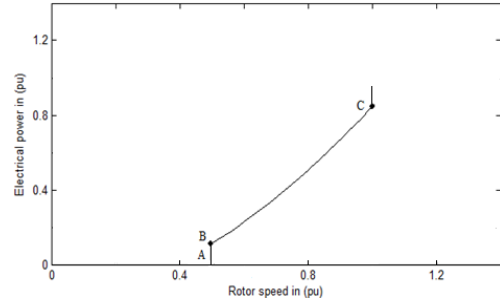


Fig. 7. Optimal output power versus rotor speed

3.7 Pitch Angle Controller

The pitch angle controller is only active in high wind speeds. The aim of this controller is to limit the output power and rotor speed to their rated values.

When the output power is below its rated value the pitch controller sets the pitch angle equals zero, since it is the optimum value for maximizing the output power. However, when the output power exceeds the rated value the pitch controller increases the pitch angle in order to decrease the performance coefficient and hence decreasing the power captured. Figure 8 shows the block diagram of the pitch angle controller. Since the pitch angle cannot change immediately due to the size of rotor blades, a rate limiter is provided. It limits the rate of change of the pitch angle to 7<sup>0</sup>/s.

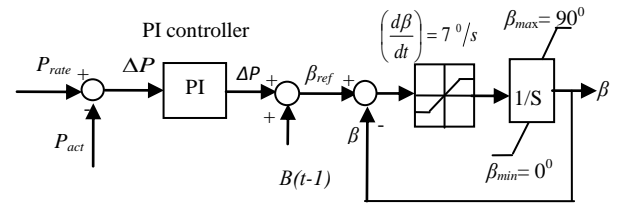


Fig. 8. Block diagram of Pitch Angle Controller.

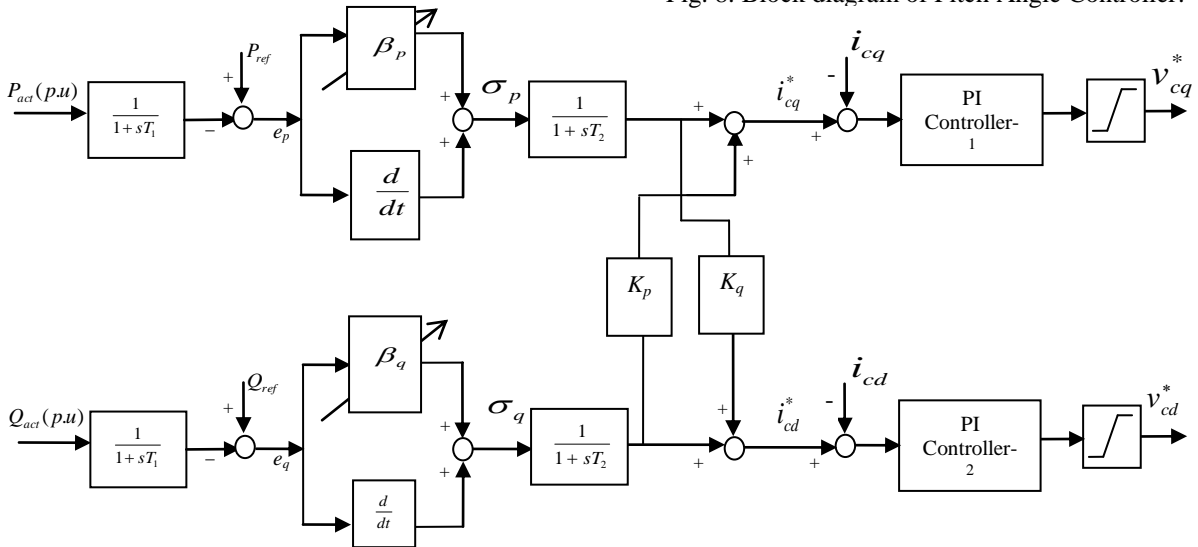


Fig. 5. Novel variable structure coordinated sliding model controller scheme with (P, Q) loop inter-coupling \*

#### 4. DIGITAL SIMULATION RESULTS

The mathematical model of the overall system has been simulated in Matlab-Simulink, with a fixed step solver of fixed step size equals to 0.001sec. The parameters of the wind turbine and the BDFM are given in Appendix B, in addition, the parameters of all controllers used are listed in Appendix C.

Different scenarios are simulated to assess the dynamic performance of both the BDFG controller and the overall control of the variable speed /variable pitch wind turbine. The dynamic response of the system is investigated when the system is subjected to different patterns of wind speed as given in following subsections.

##### 4.1 Digital Simulation Results for Wind Speeds Below its Rated Value

The simulation was carried out when the wind speed had a mean value of 9 m/s with turbulent intensity of 8 % as shown in Figure 9(a). The output active power from the power winding is shown in Figure 9 (b). It can be noticed that the fast oscillations in wind speed are filtered out from the electrical output power.

Figure 9 (c) depicts the generator speed, from which it can be seen that the generator speed follows the reference speed exactly. This assures that the generator is able to extract maximum energy from the wind. It can also be seen that the speed controller has fast response to the changes in wind speed.

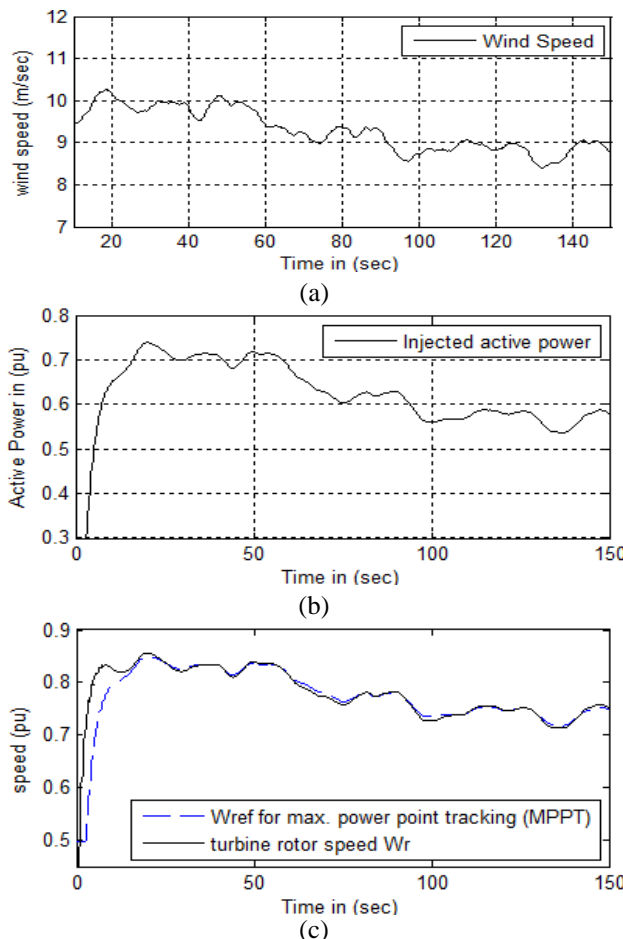


Fig. 9. Wind speed pattern for 150sec. duration (a), injected active power to the grid from the PW (b), rotor speed response and its reference (c)

Figure 10(a) depicts the tip speed ratio (TSR) of the wind turbine; it can be seen that this ratio is approximately equal to the optimal value ( $\lambda_{opt}=6.3$ ). It means that the wind turbine operates at the optimum condition. Figure 10(b) shows the value of the performance coefficient of the wind turbine. It can be noted that its value almost coincides with the optimal value of this turbine which is equal to  $Cp_{max}=0.438$ . Figure 10(c) illustrates the reactive power response and its command, in which the command reactive power was set to zero.

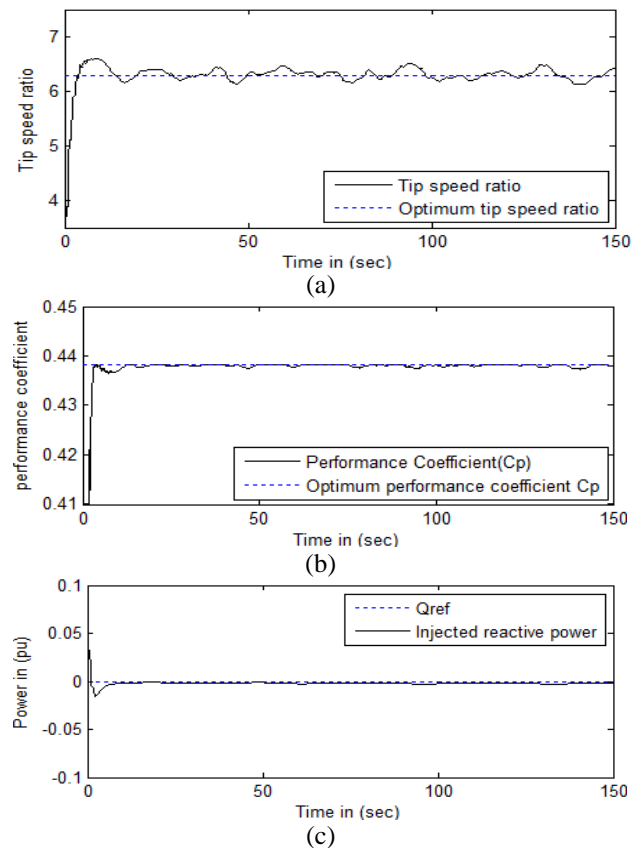


Fig. 10. Tip Speed Ratio of the wind turbine (a), performance coefficient of the wind turbine (b), reactive power response of the PW (c)

##### 4.2 Digital Simulation Results for Wind Speeds around its Rated Value

The simulation was carried out when the wind speed had a mean value of 12 m/s with turbulent intensity of 8 % as shown in Figure 11 (a), (b), (c) illustrate the output active power from the BDFG and the rotor speed respectively. It can be noticed that during the interval, at which the wind speed is larger than its rated value the speed and pitch controllers are active in order to limit the output power and rotor speed to their rated values. On the other hand when the wind speed is smaller than the rated value the speed controller only is active to maximize the output power, but the pitch controller is inactive.

Figure 11 (d) illustrates the pitch angle of the wind turbine blades. It can be seen that the pitch controller was active only in the interval, during which the wind speed is larger than the rated value. Figure 11 (e) illustrates the reactive power response.

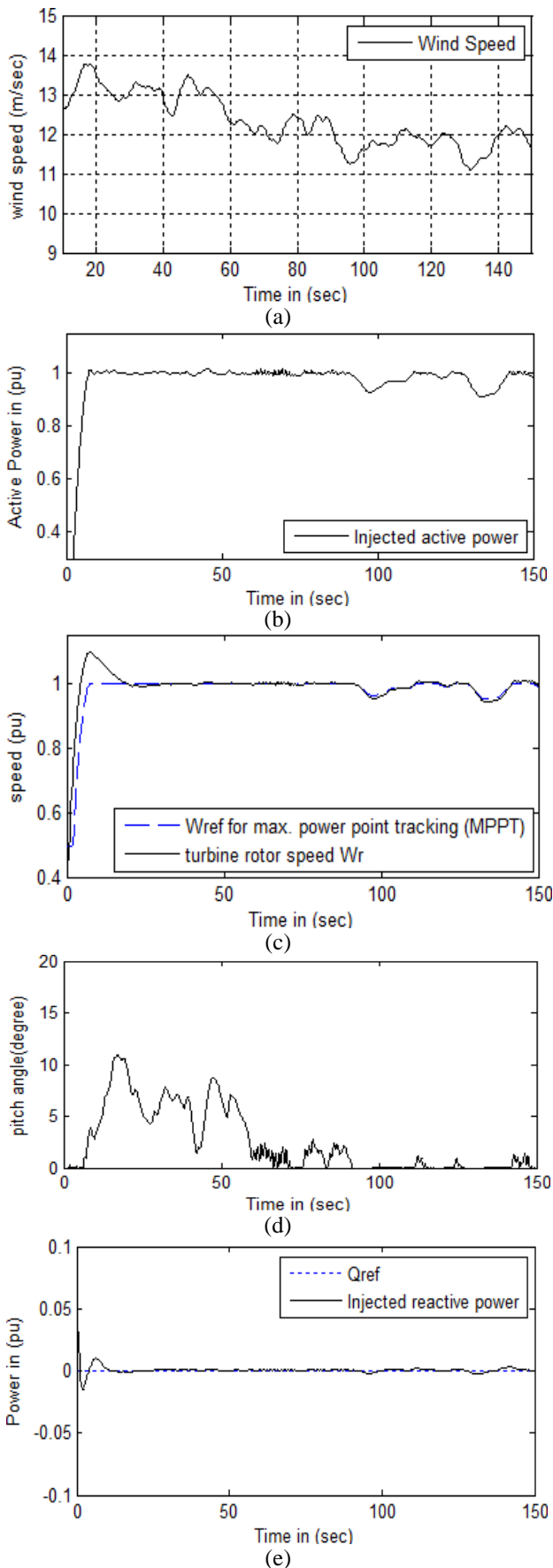


Fig. 11. Wind speed pattern for 150 s. duration (a), injected active power to the grid from the PW (b), rotor speed response and its reference (c), pitch angle (d), reactive power response of the PW (e)

### 4.3 Digital Simulation Results for Step Change of Wind Speed

The simulation results of the system under study are carried out when the system is subjected to a step change in wind speed as shown in Figure 12 (a). Figure 12 (b) depicts the dynamic response of the active power of the power winding, it can be seen that the active power response has a very small overshoot at the instance of step change of wind speed. Figure 12 (c) shows the response of the reactive power. Figure 12 (d) shows the speed response of the rotor, it can be seen that the speed of rotor follow the reference speed with small overshoots at the instance of step change.

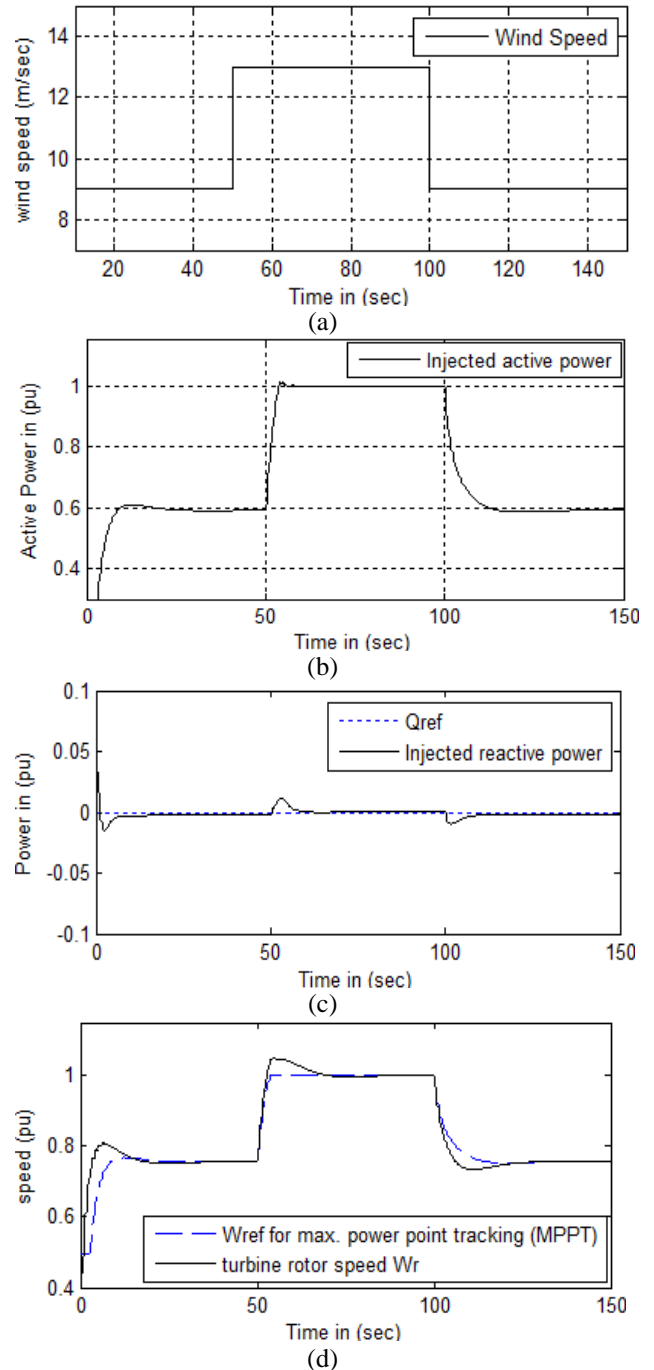


Fig. 12. Wind speed pattern for 150 s. duration (a), injected active power to the grid from the PW (b), reactive power response of the PW (c), rotor speed response and its reference (d).

### 4.3.1 Digital Simulation Results for Short Circuit Condition

The simulation results of the system under study are carried out when the system is subjected to short circuit at the generator bus. The wind speed was equal to 12 m/s. The output active power from the generator was equal to 1 pu, while the reactive power was equal to zero. The short circuit happened at  $t = 50$  s for duration of 5 cycles (0.1 s) then the fault is cleared.

Figure 13 (a) shows the transient response of the active power output from the power winding of the BDGF. It can be seen that, the power delivered from the BDGF during the fault dropped to zero then after the clearance of the fault it increased to about 1.77 pu, due to the acceleration action, then it is reduced quickly to its steady state value.

Figure 13 (b) depicts the dynamic response of the speed of the wind turbine rotor, it can be seen that at instance of sc occurrence the speed is increased to 1.058 pu, since there is no output power and the input power is absorbed by the rotating parts. Figure 13 (c) shows that the reactive power response is associated with fast oscillations and a 2 pu overshoot then it drops quickly to the same steady state value before the occurrence of the fault.

Figure 13 (d) shows the PW current, it can be seen that the PW current reached 2.1 pu during the fault, then it quickly drops to its steady state value after the clearance of the fault. Figure 13 (e) shows the transient response of the control winding current. It can be seen that this current reached 1.6 pu during the fault.

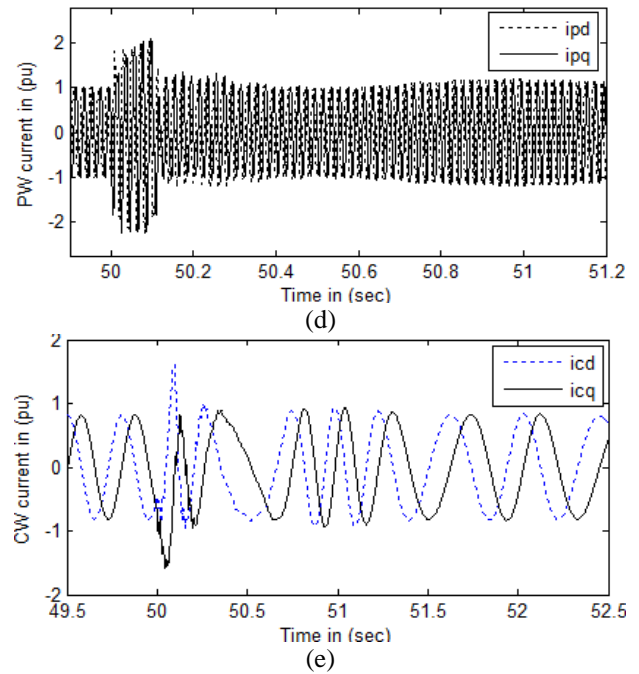
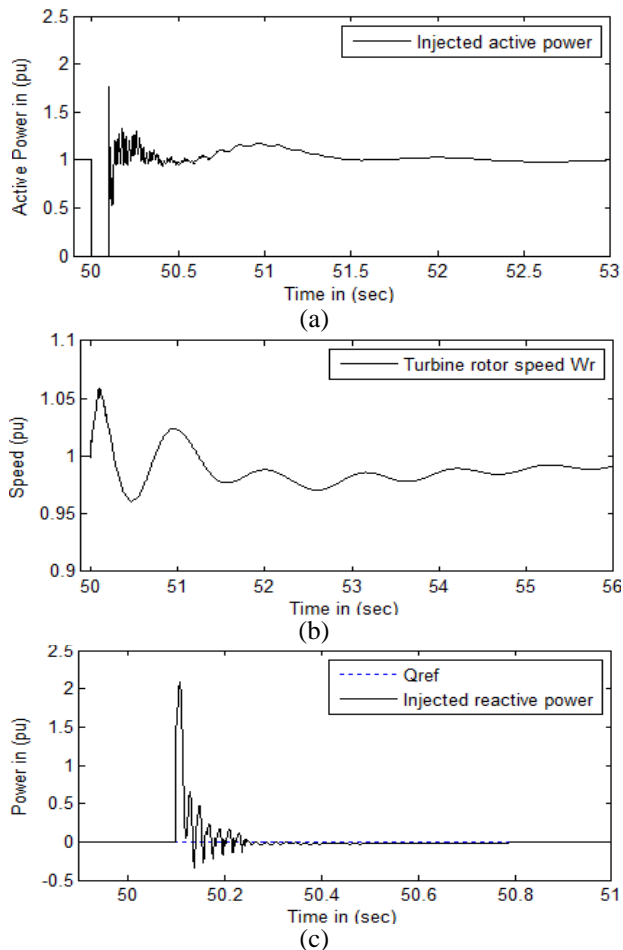


Fig. 13. Output active power from the power winding (a), speed of wind turbine (b), reactive power output from the power winding (c), power winding current in the PW reference frame (d), control winding current (e)

### 4.3.2 Digital Simulation Results for Open Circuit

The simulation results of the system under study are carried out when the system is subjected to open circuit at the generator bus. The wind speed was constant at 12 m/s, the output active power from the generator was equal to 1 pu, while the reactive power was equal to zero. The open circuit happened at  $t = 50$  s for duration of 2 cycles (0.04 s) then the generator is reconnected to the grid.

Figure 14 (a) shows the active power response of the system, it can be seen that the active power is decreased instantaneously to zero during the open circuit period and at the instance of reconnecting the generator the power is increased with under damped response with maximum overshoot of 0.7 pu, the active power is then reached to steady state value of one pu after 1.5 s.

Figure 14 (b) shows the reactive power response, it can be notice that it has a damped oscillating response with an overshoot of 1.1 pu. Figure 14 (c) depicts the speed response of the wind turbine rotor, it can be notice that at the instance of open circuit the speed is increased to about 1.04 pu, then it oscillate with damped behavior about its rated value, it reached the steady state value after 4 sec. Figure 14 (d) shows the response of the PW currents, it can be seen that the PW current decreased to zero during the open circuit interval then it return to its steady state value quickly after about 1 sec, also it can be noticed that the maximum overshoot of the PW current is 0.8 pu.

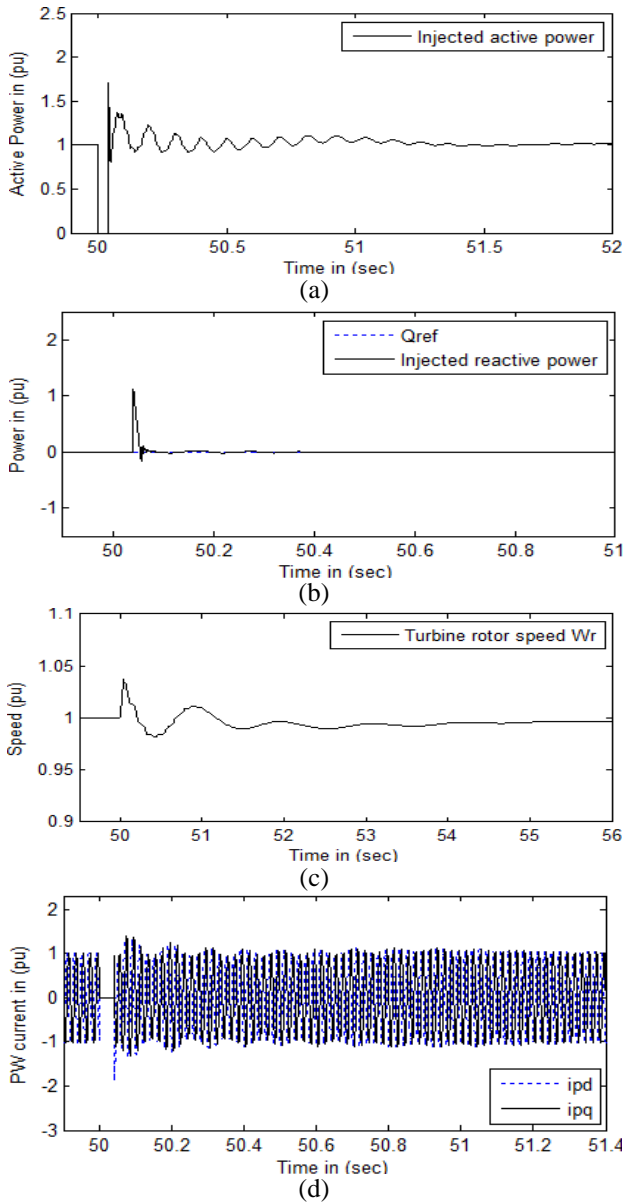


Fig. 14. Output active power from the power winding (a), Reactive power output from the power winding (b), Speed of wind turbine (c), Power winding current in the PW reference frame (d)

### 5. CONCLUSION

This paper presented a new coordinated inter-coupled variable structure controller for the brushless doubly fed induction generator (BDFG) with P, Q loop inter-coupling for the purpose of controlling its active and reactive power. The application of the novel controller for the BDFG machine is validated through simulation analysis on Matlab/Simulink program. The dynamic response of the brushless doubly fed induction generator with this proposed controller is obtained and analyzed. By inspection of the dynamic response, it can be realized that the dynamic response of the BDFG when provided with the proposed controller is improved and the power ripple is minimized in compared with that of the conventional proportional plus integral (PI) controller. The Inter-Coupled controller ensures less ripple content, fast dynamics response and enhanced dynamic fast tracking of power (P, Q) references.

### APPENDICES

#### Appendix (A)

Derivation of the dynamic relation between CW and PW current:

Equation (9) can be rearranged as follows:

$$i_r = \frac{\psi_p - L_{sp}i_p}{L_{hp}} \quad (24)$$

Substituting equation (24) into equation (13) to obtain the rotor flux as a function of the PW, the CW currents and the PW flux yields:

$$\psi_r = \frac{L_r\psi_p}{L_{hp}} + (L_{hp} - \frac{L_rL_{sp}}{L_{hp}})i_p + L_{hc}i_c \quad (25)$$

Substituting equations (24) and (25) into equation (12) and putting  $v_r=0$  then expanding the resulting equation into d-q components. Yield equations (19) and (20) which describes the dynamic relation between CW and PW currents.

#### Appendix (B)

(i) BDFG data:

$R_{sp}=1.732\Omega$	$R_{sc}=1.079\Omega$	$R_r=0.473\Omega$
$L_{sp}=714.8 \text{ mH}$	$L_{sc}=121.7 \text{ mH}$	$L_r=132.6 \text{ mH}$
$L_{hp}=242.1 \text{ mH}$	$L_{hc}=59.8 \text{ mH}$	$p_1=3$
		$p_2=1$

(ii) The wind turbine data:

Number of blades = 3      Blade radius  $R_r = 37.5 \text{ m}$   
 Turbine inertia (pu) = 2.5 s    Cut in speed = 3 m/s,  
 Cut out speed = 25 m/s  $\rho = 1.225 \text{ kg/m}^3$ ,  
 Gear box ratio 1:42

#### Appendix (C)

(i) Parameters of the novel controller:

$T1 = 0.003 \text{ s}$	$T2 = 0.001 \text{ s}$
$\beta_p = 0.7 + 5e_p$	$B_q = 0.78 + 70e_q$
$K_p = 0.1$	$K_i = 0.1$
PI controller -1 $K_p = 40, K_i = 10$ PI controller -1 $K_p = 45, K_i = 25$	

(ii) Parameters of the speed PI controller:

$K_p = 1.8$	$K_i = 0.8$
-------------	-------------

(iii) Parameters of the pitch angle PI controller:

$K_p = 20$	$K_i = 5$
------------	-----------

### References

- [1] A. D. Hansen, F. I. Poul, and F. Blaabjerg, Overall control strategy of variable speed doubly-fed induction generator wind turbine, Nordic wind power conference, 1-2 March, Chalmers University of Technology, (2004).
- [2] R. Pena, J. C. Clar, and G. M. Asher, Doubly fed induction generator using back-to-back PWM converters and its application to variable speed, IEEE Proc. Electr. Power Appl., 143(5), 380-387, (1996).
- [3] K. Protsenko, and D. Xu, Modeling and control of brushless doubly-fed induction generators in wind energy applications, IEEE Trans. Power Electronics, 23(3), 1191-1197, (2008).
- [4] M. S. Boger, A. K. Wallace, R. Spee, and R. Li, General pole number model of the brushless doubly-

- fed machine, IEEE Trans. Ind. Appl., 31(5), 1022-1028, (1995).
- [5] W. R. Brassfield, R. Spee, and T.G. Habetler, Direct torque control for brushless doubly-fed machines, IEEE Trans. Ind. Appl., 32(5), 1098-1104, (1996).
- [6] J. Poza, E. Oyarbide, and D. Roye, New vector control algorithm for brushless doubly-fed machines, Proc. IEEE IECON Conf., Seville, Spain, Vol:2, 1138-1143, November (2002).
- [7] S. O. Madbouly, H. F. Soliman, and A. M. Sharaf, A new coordinated inter-coupled vector control of brushless doubly fed wind driven induction generator, IJPEGT Journal, Issue 2, (2011).
- [8] A. M. Sharaf, W. Wang, and I. H. Altaş, A novel modulated power filter compensator for distribution networks with distributed wind energy, Int. J. Emerg. Electr. Power Syst., 8(3), 1–20, (2007).
- [9] M. E. Şahin, A. M. Sharaf, and H. İ. Okumuş, A novel filter compensation scheme for single phase-self-excited induction generator micro wind generation system, Sci. Res. Essays, 7(34), 3058–72, (2012).
- [10] J.G. Sloopweg, H. Polinder, and W.L. Kling, Representing wind turbine electrical generating systems in fundamental frequency simulations, IEEE Trans. Energy Conversion, 18(4), 516-524, December (2003).
- [11] A. Perdana, O. Carlson, and J. Persson, Dynamic response of grid connected wind turbine with Doubly Fed Induction Generator during disturbances, Nordic Workshop on Power and Industrial Electronics, Trondheim, Norway, (2004).
- [12] S. Heier, Grid integration of wind energy conversion systems, John Wiley & Sons Ltd, (1998).
- [13] Wind Turbine, Implement model of variable pitch wind turbine Matlab/Simulink, website: [www.mathworks.com](http://www.mathworks.com), (2016).
- [14] R. Li, A. Wallace, R. Spee, and Y. Wang, Two-Axis model development of cage-rotor brushless doubly-fed machines, IEEE Trans. Energy Conversion, 6(3), 453-460, September, (1991).
- [15] J. Poza, E. Oyarbide, D. Roye, and M. Rodriguez, Unified reference frame d-q model of the brushless doubly fed machine, IEEE Proc. Electr. Power Appl., 153(5), 726-734, September, (2006).
- [16] R. Carlson, H. Voltolini, F. Runcos, P. Kuo-Peng, and N. J. Batistela, Performance analysis with power factor compensation of a 75 kw brushless doubly fed induction generator prototype, Proc. IEEE IEMDC Conf., Antalya, Turkey, vol:2, 1502-1507, May, (2007).
- [17] D. Basic, J. G. Zhu, G. Boardman, Transient performance study of a brushless doubly fed twin stator induction generator, IEEE Trans. Energy Conversion, 18(3), 400-408, September (2003).

## Biographies



**Dr. Sayed O. Madbouly** is currently an assistant professor at Electric Power and Machines Department, Faculty of Engineering, Ain Shams University. He was born in Cairo, Egypt on November 28, 1975. He received his B.Sc., M.Sc. and Ph.D. degrees in Electrical Engineering from Electrical Power and Machines Department, Faculty of Engineering, Ain Shams University, Cairo, Egypt, in 1998, 2004 and 2010 respectively. His current Research areas include Electric Drives, Renewable Energy, and Artificial Intelligent Applications on Electrical Machines.

E-mail: [sayed\\_madbouly@hotmail.com](mailto:sayed_madbouly@hotmail.com)



**Prof. Adel M. Sharaf** obtained his B.Sc. degree in Electrical Engineering from Cairo University in 1971. He completed an M.Sc degree in Electrical engineering in 1976 and Ph.D degree in 1979 from the University of Manitoba, Canada and was employed by Manitoba Hydro as Special Studies Engineer, responsible for engineering and economic feasibility studies in Electrical Distribution System Planning and Expansion. Prof. Sharaf was selected as NSERC-Canada research-assistant professor in 1980 at University of Manitoba. He joined the University of New Brunswick in 1981 to start a tenure-track academic career as an Assistant professor and he was promoted to Associate Professor in 1983, awarded tenure in 1986, and the full professorship in 1987. Dr. Sharaf has extensive industrial and consulting experience with Electric Utilities in Canada and Abroad.

E-mail: [profdramsharaf@yahoo.ca](mailto:profdramsharaf@yahoo.ca)